

## Structural changes in $\text{ZrO}_x\text{N}_y/\text{ZrO}_2$ coatings deposited through spray pyrolysis-nitriding

G. I. Cubillos<sup>a</sup>, J. J. Olaya<sup>b</sup>, M. Bethencourt<sup>c</sup>, G. Cifredo<sup>d</sup> and G. Blanco<sup>d</sup>

<sup>a</sup>*Departamento de Química, Facultad de Ciencias,  
Universidad Nacional de Colombia, Cra 30 No 45-03. Bogotá-Colombia,  
e-mail: gcubillos@unal.edu.co*

<sup>b</sup>*Departamento de Ingeniería Mecánica y Mecatrónica, Facultad de Ingeniería,  
Universidad Nacional de Colombia, Bogotá-Colombia,  
e-mail: jjolayaf@unal.edu.co*

<sup>c</sup>*Materials Science and Metallurgical Engineering Department, and Inorganic Chemistry Department,  
University of Cádiz, Marine Science and Technology Center of Andalucía,  
International Campus of Excellence of the Sea (CEI-MAR),  
Avda. República de Saharaui, Puerto real, E-11510. Spain.  
e-mail: manuel.bethencourt@uca.es*

<sup>d</sup>*Departamento de Ciencia de los Materiales e Ingeniería Metalúrgica y Química Inorgánica, Facultad de Ciencias,  
Universidad de Cádiz, Campus Río San Pedro, 11510-Puerto Real, Cádiz, Spain.  
e-mail: gustavo.cifredo@uca.es; ginesa.blanco@uca.es*

Received 27 November 2013; accepted 28 March 2014

Thin films of zirconium oxynitride were deposited on stainless steel 316L and characterized through ultrasonic spray pyrolysis-nitriding (UPS-N). Initially, thin films of  $\text{ZrO}_2$  are deposited using ultrasonic spray pyrolysis, and later  $\text{ZrO}_2$  films were nitrided in a  $\text{NH}_3$  atmosphere. We analyzed the effect of some variables, such as substrate temperature, flow ratio, and time of the production of coatings and their influence on the structure of the films. The characterization was carried out using X-ray diffraction (XRD) spectroscopy, X-ray photoelectron (XPS), and scanning electron microscopy (SEM).

Films that were grown using the UPS method exhibited a tetragonal zirconia polycrystalline structure with preferential orientation in plane (101). These films, after being nitrided in an atmosphere of anhydrous ammonia at 1023 K, go through two processes: a phase transition from tetragonal to monoclinic, and later the formation of zirconium oxynitride rhombohedral  $\text{ZrO}_x\text{N}_y$ .

**Keywords:** Zirconium oxynitride; spray pyrolysis; coatings.

PACS: 61.66.Fn; 61.05.cp; 68.37.Ps; 67.80 dm

### 1. Introduction

Metal/ceramic composites have become a focus of research because they can meet service requirements not met by metal or ceramic independently and have the advantage of combining the desirable properties of metal with the chemical inertness, high degree of temperature resistance, and hardness of ceramics. They are potential materials for applications in extreme temperature and corrosive environments. The process usually employed to manufacture such materials involves making contact between the ceramic plate and the metal plate so that a high pressure ceramic diffuses on the metallic material and subsequently sinters at temperatures above 1573 K to ensure the inclusion of the two materials by decreasing the maximum occurrence of fractures in the ceramic, generated by the difference in ductility of both. However, the process has problems, such as rolling, breakage, and detachment of the ceramic, reducing the range of applications of these types of materials, such as fuel cells, oxygen sensors, refractory, catalysts, and corrosion resistance materials [1-7].

Other methods used in the production of metal-ceramic materials consist of depositing the ceramic coating on the metal, either using physical techniques such as vapor depo-

sition (PVD), or through chemical techniques such as sol-gel or spray pyrolysis. In spray pyrolysis, a dissolved solute transported by a gas stream, which may be inert or reactive, thermally decomposes upon touching a hot substrate. Chemical transformation occurs when the precursor is deposited on the substrate surface, or may be performed by subsequent heating of the dew [8-11]. Once the precursor is spread on the heated surface, the solvent evaporates and the product of the chemical decomposition interacts with the substrate. The film formation depends on the size of the drop, the reaction, and the evaporation of the solvent [9].

The process used for depositing the ceramic material on the metal determines the properties, structure, and growth the coating. Coatings extend the service life of the substrate, which is closely related to its properties and the environment in which the material is used. When creating an interface in which materials of different natures are involved, such as metal and ceramics, changes occur in some of their properties, due to the chemical nature of the two materials. Crystallographic changes can occur because of the difference between the crystal structure of the deposited metal and the ceramic; electronic changes because the ceramic exhibits an

ionic-covalent bond, where the electron motion is restricted, while in metallic bonding the electrons are in constant motion; changes in the mechanical and thermo-mechanical properties because of the difference in the thermal expansion coefficients, which are higher in metals; and finally in some cases thermodynamic changes, where the possibility of forming reaction products at the interface exists [12,13].

The case of doping of zirconia with aliovalent cations  $Y^{3+}$ ,  $Ce^{3+}$ ,  $Fe^{3+}$ ,  $Cr^{3+}$ ,  $Co^{2+}$ ,  $Ni^{2+}$ ,  $Cu^{2+}$ ,  $Ca^{2+}$ , and  $Zn^{2+}$  has been extensively investigated [14-16]; however, doping with aliovalent anions is less frequent. The results in this field show that the introduction of nitrogen into the crystalline structure of  $ZrO_2$  gives it the characteristics of a semiconductor, increasing its hardness and corrosion resistance [17].

This type of nitrogen doping on transition metal oxides gives rise to so-called transition metal oxynitrides, which combine the ionic character of the oxide with the nitride covalent character, generating a new material with substantially different properties, such as fracture toughness and oxide ion conductivity [18-20]. Unlike aliovalent cation doping, where there is completely random replacement, replacement of oxygen with nitrogen in the crystal structure of the zirconia can easily display an array in which the formation of a fluorite-type structure predominates, organized to form a super network [21].

Various crystalline phases of zirconium oxynitride ( $ZrO_xN_y$ ) have been identified according to the synthesis method employed: in the temperature range 1173 to 2273 K, the so-called phase  $\gamma$  ( $Zr_2N_2O$ ), phase  $\beta$  ( $Zr_7N_4O_8$ ), phase  $\beta'$  ( $Zr_7N_{3.2}O_{9.2}$ ), and between 1673 and 2273 K in a nitrogen atmosphere phase  $\beta''$ , similar to phase  $\beta'$ . Phase  $\gamma$ - $Zr_2N_2O$  has a cubic structure with lattice parameters similar to those of  $ZrO_2$  (c), and phases  $\beta$  ( $\beta$ ,  $\beta'$ ,  $\beta''$ ) show a slight trigonal distortion of the cubic phase. Anion vacancies are ordered along the c axis, and for each phase trigonal  $\beta$  he positions are different [22,23].

This paper presents an optimization of the nitriding process in an anhydrous ammonia atmosphere of tetragonal zirconia films [ $ZrO_2$  (t)] deposited on stainless steel AISI 316L through the spray pyrolysis method with previously stan-

dardized conditions [24] to produce zirconium oxynitrides  $ZrO_xN_y$  at 1023 K. The structural transformation of  $ZrO_2$  (t) to  $ZrO_xN_y$  is studied, and its composition is confirmed through XPS.

## 2. Materials and methods

### 2.1. Substrate preparation

Plates of AISI 316L stainless steel  $2.0 \times 2.0$  cm in area, polished with SiC 80, 120, 240, 400, 600, 1500, and 2500 grit were used. Organic impurities were removed prior to deposition by washing with three solvents of different polarity, dichloroethane, acetone, and isopropanol, for 3 min using ultrasound.

### 2.2. Spray pyrolysis deposition conditions

For the deposition of zirconia, conditions previously standardized by G. I. Cubillos *et al.* [24] were used. The film is deposited through the thermochemical transformation of a solution of zirconium acetylacetonate/Yttrium nitrate (III):  $Zr(C_5H_7O_2)_4$  0.025M -  $Y(NO_3)_3 \cdot 6H_2O$   $7.0 \times 10^{-4}$  M of Sigma-Aldrich Chemicals in methanol 99.9%. Transport was carried out with aerosol generated by an ultrasonic nebulizer at 256 MHz, using drag flow at 3.0 L/min. and direction flow at 0.80 L/min.

The nitriding conditions of zirconia in an anhydrous ammonia atmosphere at atmospheric pressure were subsequently chosen. For this, various conditions of temperature, time, and flow of anhydrous ammonia were assayed. The conditions tested are shown in Table I.

Having established the optimal conditions for the nitriding of zirconia, the samples of AISI 316L stainless steel coated with zirconia were nitrided in an anhydrous ammonia atmosphere at 1023 K for 30 h. The cooling was performed slowly in flowing ammonia to promote the accommodation of the stresses that are generated at the interface due to the difference between thermal expansion coefficients of the materials and prevent possible oxidation of the coating during that process.

TABLE I. Nitriding conditions tested for zirconia films.

Temp. K	4 h	7 h	10 h	15 h	20 h	25 h	10	20	25	30
							L/min	L/min	L/min	L/min
							$\Phi NH_3$ 30 L/min			
							t= 30 h			
723	•	•	•	•						•
773	•	•	•	•						•
873	•	•	•	•						•
973	•	•	•	•						•
1023	•	•	•	•	•	•	•	•	•	•
1073				•						•

### 2.3. Characterization of the coatings

The structural characterization of the films was performed via X-ray diffraction (XRD) with X-pert Pro Panalytical diffractometer operating at 30 kV and 20 mA with  $\text{Cu K}\alpha$  radiation 1.540998 Å, current of 49 mA and potential difference of 45 kV. The sweep range was  $10^\circ$  to  $100^\circ$  with step size  $0.02^\circ$  in continuous mode. The surface morphology was characterized by imaging the secondary electrons using a Quanta 2000 scanning electron microscope operating at 15 kV and 10 mA. Atomic force microscopy was performed using a Park Scientific Autoprobe CP instrument with a study area of  $25 \mu\text{m}^2$  and frequency of 10 Hz. The complexity of the phase mixture  $\text{ZrO}_2(m)$ ,  $\text{ZrO}_2(t)$ ,  $\text{ZrO}_x\text{N}_y$ , and austenite made phase identification difficult, and therefore it was necessary to determine the phases present in both the substrate and the film with the program EVA Socabim, using ICDD database PDF-2 and in some cases the Rietveld refinement program Fullprof [25]. Chemical composition of the zirconium oxynitride coatings was determined through X-ray photoelectron spectroscopy (XPS). XPS spectra were obtained with a Kratos Axis Ultra DLD instrument, equipped with a monochromatized  $\text{Al K}\alpha$  x-ray source (1486.6 eV), which was operated with selected x-ray power of 150 W. XPS spectra were obtained in the Constant Analyzer Energy mode (CAE), with pass energy of 20 eV for the high resolution spectra. Charging effects were compensated through low energy electron flow from the specific Kratos coaxial neutralization system. Binding Energy (BE) scale was corrected with respect to the adventitious C 1s signal at 284.8 eV. Depth profiles were obtained by using a Kratos Minibeam I ion source. Each sputtering cycle consisted of  $\text{Ar}^+$  etching at 4 kV, 20 mA (beam energy 4 keV), with raster size of  $2 \times 2 \text{ mm}^2$ .

## 3. Results and discussion

### 3.1. Phase identification

Nitriding of  $\text{ZrO}_2(t)$  deposited on stainless steel with the spray pyrolysis method was carried out in an atmosphere of ammonia in order to induce solid phase reaction  $\text{N}_2/\text{ZrO}_2$ , partially replacing oxygen with nitrogen, thereby obtaining a film of  $\text{ZrO}_x\text{N}_y$  on steel.

For studying the nitriding of the zirconia layer deposited on steel, an initial temperature of 723 K was used. It is known that in the presence of iron oxide  $\text{Fe}_2\text{O}_3$  and  $\text{Fe}_3\text{O}_4$ , the breaking of the ammonia molecule begins at 623 K [26], so a ferritic steel cylinder was used as a reactor. The process was carried out in a continuous flow of anhydrous ammonia at atmospheric pressure, in order to shift the chemical equilibrium towards the generation of nitrogen. Continuous discharge of hydrogen has the additional advantage of avoiding steel embrittlement through the action of the hydrogen that is a product of the reaction [27]. Monitoring of the reaction was carried out using X-ray diffraction following the structural change generated in the coating. This technique

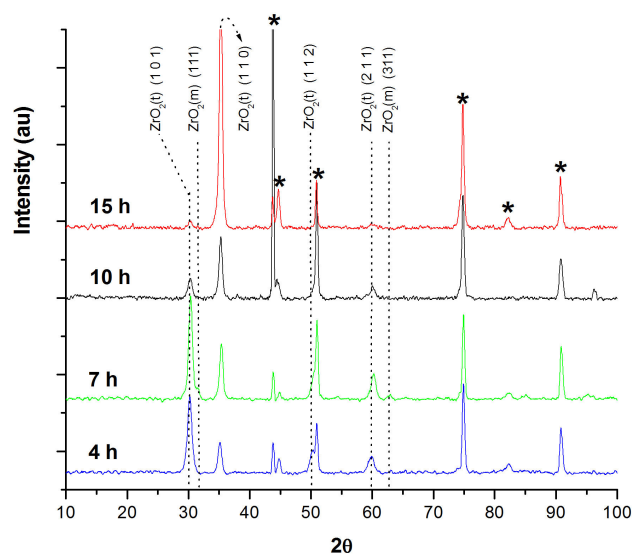


FIGURE 1. XRD patterns recorded from  $\text{ZrO}_2$  film nitrided at 873 K,  $\Phi\text{NH}_3 = 30 \text{ L/min}$ . Nitriding time: 4, 7, 10 and 15 h. AISI 316 L substrate. \*Steel phases.

allows revealing changes in the zirconia phase and the onset of oxidation and/or nitriding of the steel, and identifies some  $\text{ZrO}_x\text{N}_y$  phases, although in some cases it does not allow definitively establishing the formation of  $\text{ZrO}_x\text{N}_y$ , so the chemical composition was determined using XPS.

The nitriding treatment was carried out at constant ammonia flow of 30 L/min in the range of 723–1073 K. XRD study showed that at and below 873 K (data not shown), after 4–15 h of nitriding, phases of  $\text{ZrO}_x\text{N}_y$  were not detected (Fig. 1). At 873 K and 4 h after heating, the structure of tetragonal zirconia was stable; 7 h later, phase transformation from  $\text{ZrO}_2(t)$  to  $\text{ZrO}_2(m)$  was seen, as shown by the signal at  $2\theta = 31^\circ$  corresponding to plane (111)  $\text{ZrO}_2(m)$  and  $2\theta = 62.5^\circ$  to plane (311) of  $\text{ZrO}_2(m)$ . After 10 h of reaction, the film develops the tetragonal phase at the expense of the monoclinic form, with preferential growth of plane family (110) of  $\text{ZrO}_2(t)$ . These results show that the heat treatment at this temperature in an atmosphere of  $\text{NH}_3/\text{N}_2/\text{H}_2$  provides conditions for migration and reorganization of species on the plane (110)  $\text{ZrO}_2(P)$ . If the nitriding process is performed for 15 h at 873 K, the peak (110)  $\text{ZrO}_2(t)$  growth changes, but there is no evidence of the occurrence of phases of  $\text{ZrO}_x\text{N}_y$ .

After 30 h of treatment at 873 and 973 K (Fig. 2), the destabilization of the tetragonal phase and the simultaneous appearance of  $\text{ZrO}_2(t)$  and  $\text{ZrO}_2(m)$  were observed. This prolonged heat treatment promotes structural rearrangement, and upon raising the temperature to 1023 K, a signal  $2\theta = 18.4^\circ$  related to the planes (110) of the rhombohedral phase  $\text{Zr}_7\text{O}_8\text{N}_4$  (JPSD 00-050-1172) is observed, and, although overlapping peaks of other phases, another peak of  $\text{Zr}_7\text{O}_8\text{N}_4$  at  $2\theta = 30^\circ$ , corresponding to planes (211), which has been developing starting from 823 K, can be seen. DRX obtained in the temperature range studied is shown in Fig. 2, together with an expansion of a 1023 K diffractogram recorded between  $2\theta = 16\text{--}19^\circ$ . Signal  $2\theta = 17.6$  corresponds

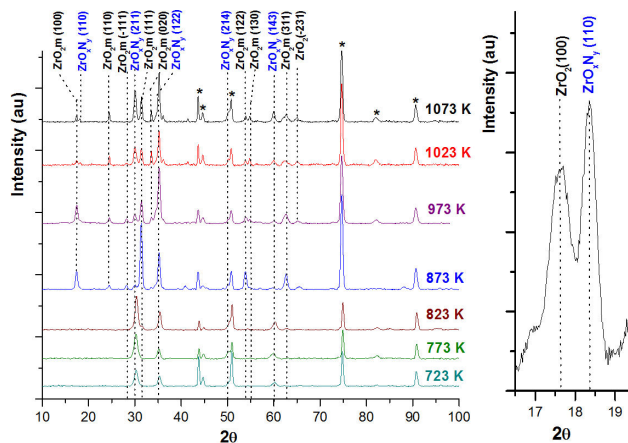


FIGURE 2. XRD patterns recorded from  $ZrO_xN_y$  film deposited on AISI 316 L substrate nitrided at different temperatures.  $\Phi NH_3 = 30$  L/min, time nitriding 30 h.

to the plane (100)  $ZrO_2$  (*m*) or baddeleyite (JPDS 00-001-0750). Between 1023 and 1123 K, no appreciable change in the phases is evident.

Diffraction signals for  $ZrO_xN_y$  and  $ZrO_2$  (*t*) are very close to each other, since the variation in the ionic  $O^{2-}/N^{3-}$  volume is very small and therefore the replacement of oxygen with nitrogen atoms leads to no detectable distortion in the  $ZrO_2$  structure. Additionally, the characteristic diffraction signals that are recorded for oxynitride at  $2\theta = 12^\circ$  and  $18^\circ$  [28] are of very low intensity,  $I=1$  to  $I=5$ . Furthermore, in some samples nitrided at 1023 K (a, c, d in Fig. 3), comparing spectra peaks with  $Zr_7O_8N_4$  (JPDS 00-048-1637), diffraction signals of steel at 74.3 and 82 degrees could be increasing due to the formation of oxynitride, since they are closer to those of 74.343 ( $I = 12.0$ ) and 81.986 ( $I = 19.0$ ) characteristic of  $ZrO_xN_y$ . Figure 3 also appears to imply that the higher the ammonia flow the greater the degree of the nitriding and the formation of ordered zirconium oxynitride.

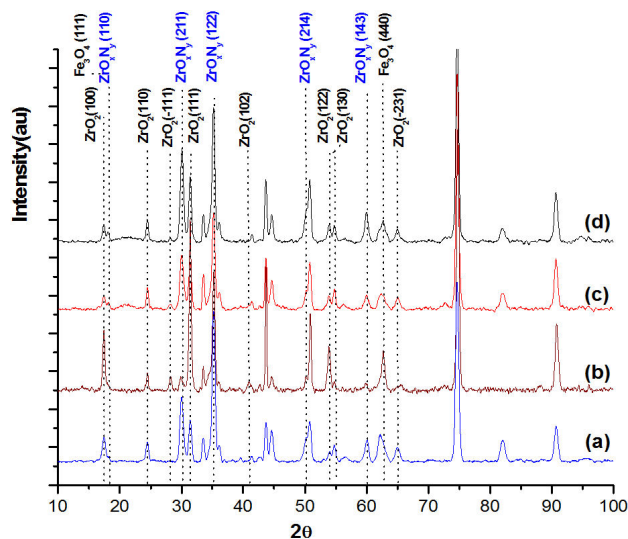
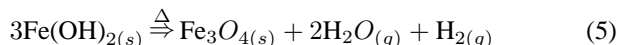
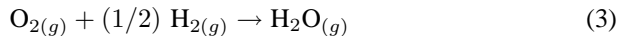
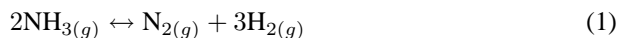


FIGURE 3. XRD patterns recorded from  $ZrO_xN_y$  film deposited on AISI 316 L substrate. Ammonia flow variable,  $\Phi NH_3 =$  a. 10, b. 20, c. 25 y d. 30 L/min. Nitriding time 30 h, temperature 1023 K.

From the spectra of the X-ray diffraction it was found that the crystalline structure of zirconium oxynitride most likely is  $Zr_7O_8N_4$  (JPDS 00-050-1172), and Rietveld analysis allowed confirmation of this. Results obtained are shown in Figs. 4 and 5. In Fig. 4, phases of the coating and the substrate have been identified using the Socabim EVA program with ICDD database PDF-2. Phases identified in the substrate are: ●  $FeCr_{0.29}Ni_{0.16}Co_{0.06}$ , ●  $Cr_{1.3}Fe_{0.7}O_3$ , 7O3 and cubic magnetite ●  $Fe_3O_4$  01-089-0951. The first two characteristics correspond to stainless steel, while the magnetite is oxidation redoubt formed from the reaction of iron into steel with nascent oxygen during the nitriding. In the coating, there are two distinct phases of zirconium oxynitride ●  $Zr_7O_8N_4$ , ●  $Zr_7O_{11}N_2$  and two of zirconia ●  $ZrO_2$  (*t*), ●  $ZrO_2$  (*m*).

While nitriding reaction is carried out in a reducing environment, the presence of magnetite ( $Fe_3O_4$ ) is a product of the oxidation of the substrate. At 1023 K, partial substitution of oxygen is indeed favored with nitrogen atoms in the crystal structure of zirconia, which leads to the formation of oxynitride. Released oxygen reacts with hydrogen from the lysing of  $NH_3$  (g), forming water molecules in the vapor phase that can oxidize iron to magnetite. The series of reactions 1-5 illustrates the process [29,30].



The EVA program, which searches the database ICDD PDF-2, and the simulation of the experimental diffractogram using the Rietveld program allow discriminating the stages proposed by EVA. For this, the positions of  $Ce_7O_{12}$  [31] and the parameters of the network settings for  $Zr_7O_8N_4$  JPDS00-50-1172 were taken as the initial atomic positions for  $Zr_7O_8N_4$ . Isoelectronic ions  $O^{2-}$  of  $N^{3-}$  were not distinguished. Anion positions were not refined, keeping the initial ones. The position of the Zr 18f was refined with respect to the initial position of the Ce. In the setting it was found that refined crystallographic parameters do not differ substantially from those initially supposed. Refined positions of Zr are:  $x = 0.42814$ ,  $y = 0.13118$ ,  $z = -0.02816$ , and refined lattice parameters are:  $a = 9.587042$  and  $c = 8.950155$ , results quite similar to the original, with a deviation of 0.51% in *a*, and 1.13% in *c*. The fit obtained is shown in Fig. 5. Square chi of 2.502, resulting in little difference between the experimental diagram (red) and the simulated one (black), allows confirming that the simulation is good enough to verify the structural identification. So it is confirmed that the coating is mainly formed by a mixture of phases:  $ZrO_2$  (*m*) and oxynitride rhombohedral  $Zr_7O_8N_4$ , the first being the major component.

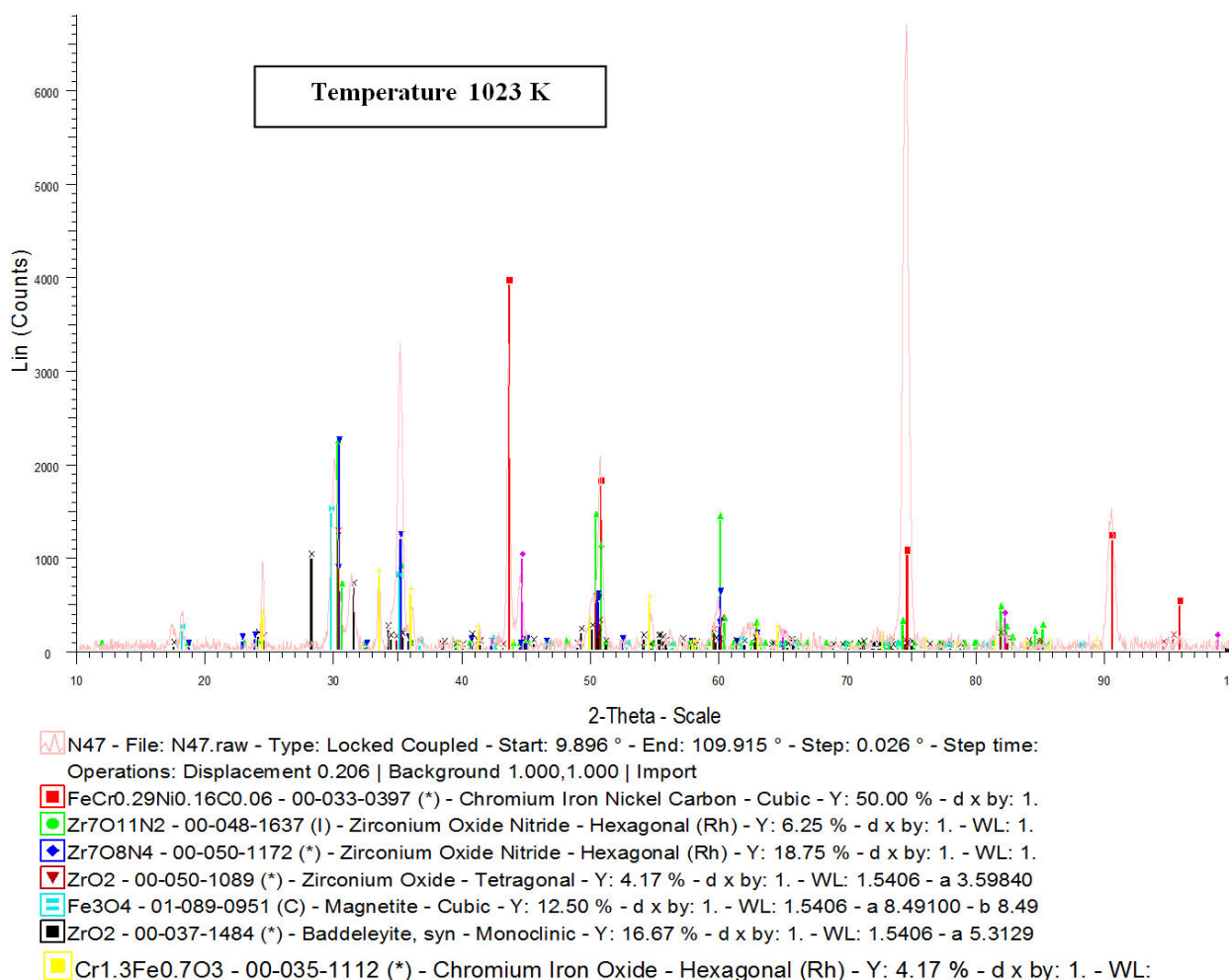


FIGURE 4. Identification of the phases using the program EVA from Socabim, with the data base ICDD PDF-2 for the coating and AISI 316 L nitride at 1023 K,  $\Phi_{NH_3} = 30$  L/min, time of nitriding 30 h.

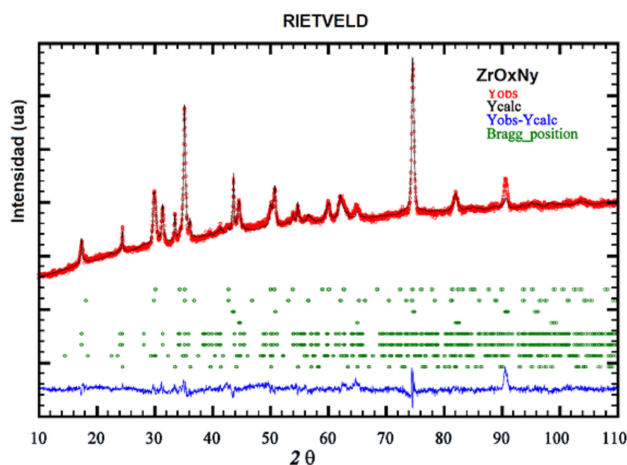


FIGURE 5. Rietveld refinement for coating of  $ZrO_xN_y$  nitrided at 1023 K,  $\Phi_{NH_3} 30$  L/min, time 30 h.

Nitriding of  $ZrO_2$  needs strong energy conditions to carry out substitution of oxygen with nitrogen: high temperature (1023 K), 30 h of reaction, and high anhydrous ammonia flow (30 L/min). From a thermodynamic point of view, by com-

paring Gibbs free energy ( $\Delta G_f^\circ$ ) between zirconia and nitride,  $ZrO_2$  is much more stable than  $ZrN$ . Gibbs free energy for zirconia is  $\Delta G_f^\circ = -1020$  KJ/mol [32], while for nitride it is approximately  $\Delta G_f^\circ = -315$  KJ/mol. Replacing oxygen atoms in the very stable zirconia structure means breaking it out of that state and inducing a new structural rearrangement by means of strong energy conditions and a high concentration of nitrogen capable of diffusing through the surface and displacing oxygen from its equilibrium state. Moreover, during anionic substitution electroneutrality of the molecule must be maintained without modifying the cationic network, as shown by the similarity of the diffraction signals between  $ZrO_2$  (*t*) and  $Zr_7O_8N_4$ . During the process, three oxygen atoms are replaced by two nitrogen atoms ( $2N^{3-} \rightarrow 3O^{2-}$ ).

Forming rhombohedral phase zirconium oxynitride  $Zr_7O_8N_4$  requires 7 molecules of  $ZrO_2$  and two molecules of nitrogen:



To form this structure, 4 nitride anions enter, each with 3 negative charges ( $4 \times 3^- = 12^-$ ), and the six oxygen anions

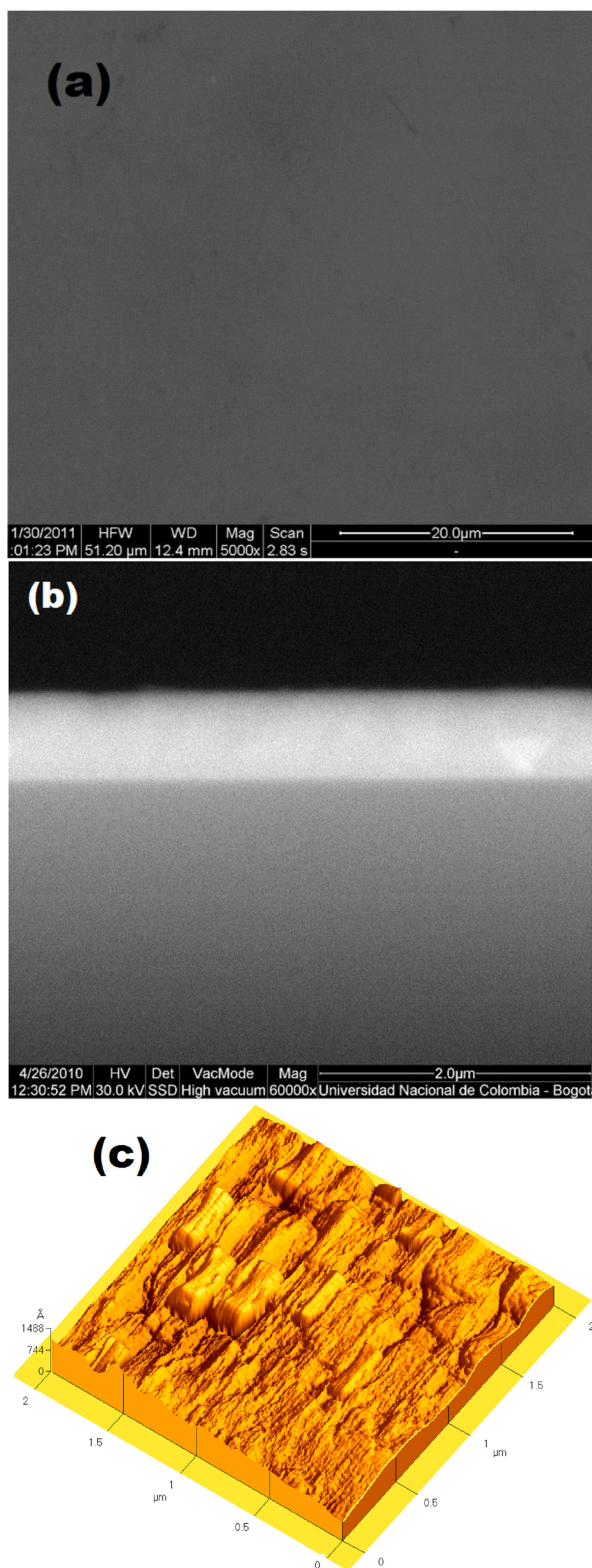


FIGURE 6. a) SEM micrograph that shows the morphology of the coatings  $ZrO_xN_y$ , b) SEM micrograph of transversal section of zirconium oxynitride film deposited on Si (100) and c) AFM micrograph of the  $ZrO_xN_y$  film deposited on stainless steel AISI 316 L film. Thin-film deposition at 1023 K, 30 h of reaction; and flow ratio  $\Phi_{NH_3} = 30$  L/min.

must be expelled ( $6x2^- = 12^-$ ) in order to maintain the electrical neutrality of the molecule, so that 6 anions  $O^{2-}$  of 14 are replaced by 4 anions of  $N^{3-}$ , as shown in Eq. (7):



This phase is almost cubic; its lattice constants exhibit a phase that is a little distorted [33].

### 3.2. Morphology

In standardized conditions for the synthesis of thin films of  $ZrO_xN_y$  using the spray pyrolysis method and nitriding, homogeneous films are obtained, as shown in the scanning electron microscopy micrograph of Fig. 6a, with a thickness of about 600 nm, as shown in the cross section cut for a coating of  $ZrO_xN_y$  deposited on a silicon wafer (100) in Fig. 6b, average roughness 135 Å, and particle size 1260 Å, as determined by AFM (Fig. 6c).

### 3.3. Composition

Chemical analysis of the surface was performed through Photoelectron Spectroscopy X-ray (XPS); chemical composition was determined at the surface and was performed by depth profile after a bombardment with  $Ar^+$  at time lapses between 1 and 245 min. This process is performed in order to obtain a profile of the coating composition and evaluate whether it is homogeneous. We found that within the temperature range between 723 and 973 K there is no nitrogen substitution in the crystal structure of zirconia, and the chemical composition of the coating is  $ZrO_2$ . As had been shown from the structural study in this temperature range, there is only one phase transition of  $ZrO_2$ , from tetragonal to monoclinic. By raising the temperature to 1023 K, a mixture of zirconium oxide and zirconium oxynitride is found, wherein the component with the highest concentration is zirconia. The depth profile of the nitrated samples at 1023 K shows that the coating surface has been oxidized to  $ZrO_2$  because it is most exposed to the action of the atmospheric oxygen. After cleaning the surface under an  $Ar^+$  atmosphere for 1 min, the coating composition is  $ZrO_2$ - $ZrO_xN_y$ . These results confirm those previously presented from the Rietveld refinement.

High resolution spectra for Zr 3d and O1s for the coating surface without sputtering are shown in Fig. 7a. Binding energies for Zr  $3d_{5/2}$  at 181.4 eV and  $3d_{3/2}$  at 183.8 eV have been identified as zirconia by several authors [34-38]. The absence of nitrogen and the 529.6 eV signal associated with O1s allow confirming that it is zirconia (Fig. 7b). Binding energy at 531.2 eV has been assigned to the species Zr-O [23,38]; binding energy for oxygen 1s at 532.2 eV in same figure has been assigned by different authors to the union (N-O) or -OH [39-41]. The absence of nitrogen in the XPS profile allows assigning it to the species hydroxyl (-OH) on the surface. These generally are associated with zirconia, because of its ability to act as a Lewis acid [42].

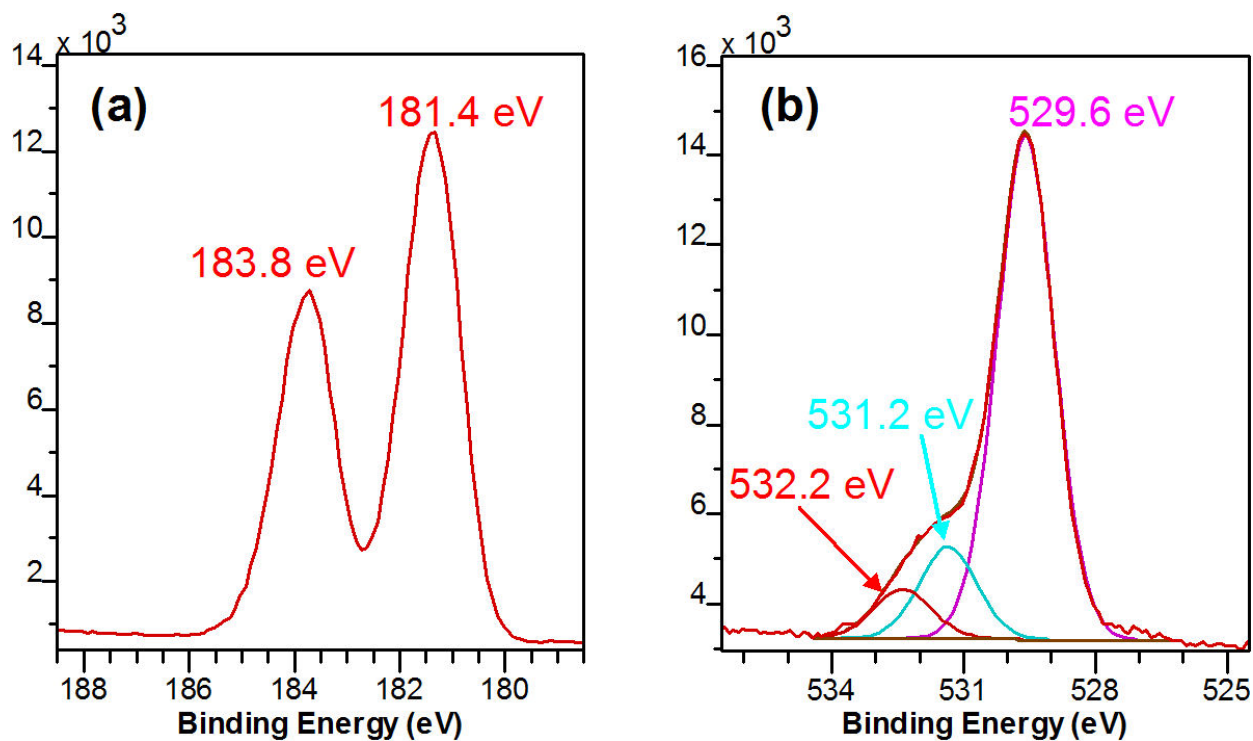


FIGURE 7. High-resolution XPS spectral analysis for the surface of  $ZrO_xN_y$  films in stainless steel. Nitrided at 1023 K,  $\Phi NH_3 = 30$  L/min nitriding time 30 h. (a) Zr3d, (b) O1s.

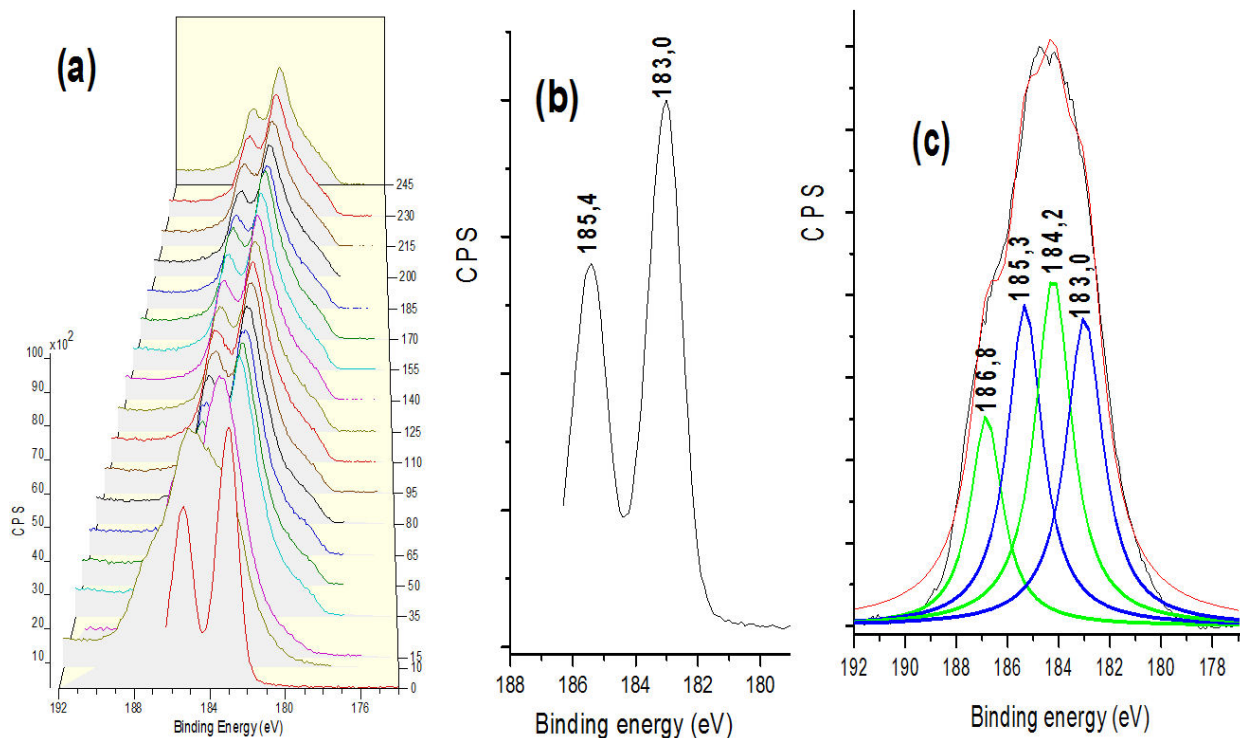


FIGURE 8. High-resolution XPS spectral analysis for the Zr3d in  $ZrO_xN_y$  (t) films, nitride at 1023 K,  $\Phi NH_3 = 30$  L/min nitriding, time 30h. (a) depth profile, (b) surface, (c) after a bombardment with  $Ar^+$  at 97 min.

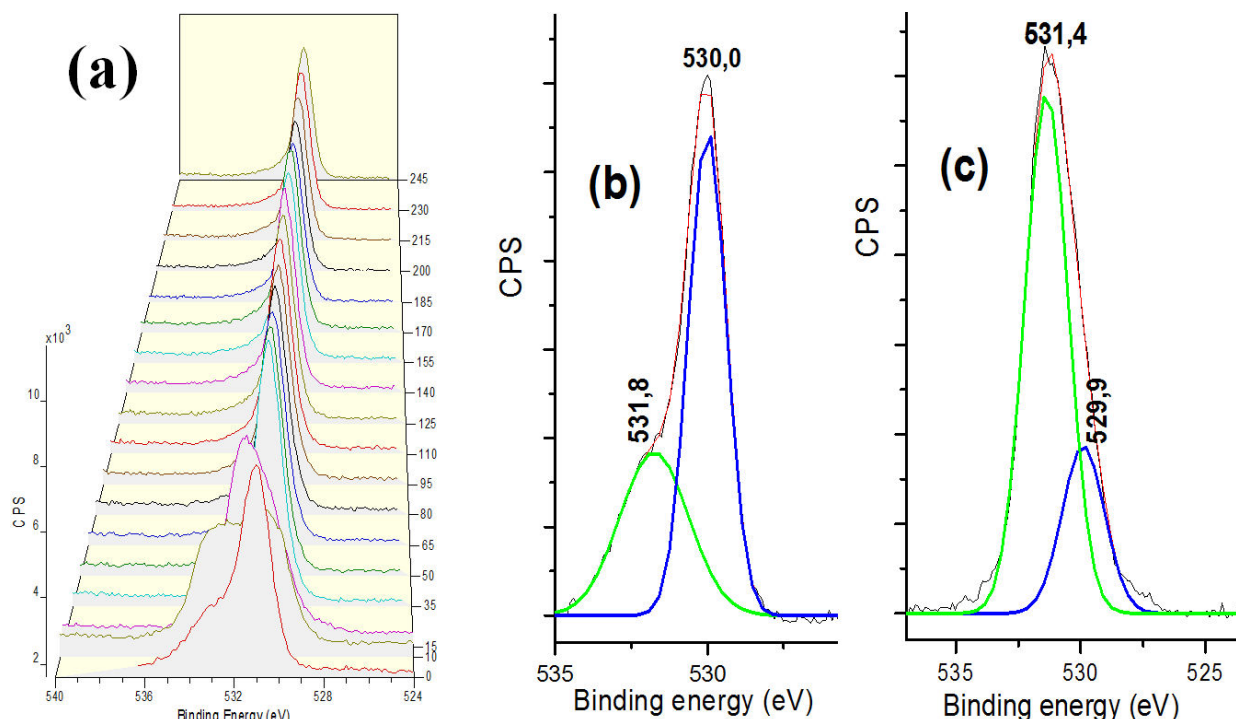


FIGURE 9. High-resolution XPS spectral analysis for the O1s in  $ZrO_xN_y$  (t) films, nitride at 1023 K,  $\Phi NH_3 = 30$  L/min nitriding, time 30h. (a) depth profile, (b) surface, (c) after a bombardment with  $Ar^+$  at 97 min.

The depth profile for Zr 3d in Fig. 8a shows that near the coating surface binding energies are predominantly zirconia, in Fig. 8b the two predominant XPS peaks around  $3d_{5/2}$  de 183.0 eV and  $3d_{3/2}$  de 185.4 eV in the Zr 3d spin-orbit doublet para  $ZrO_2$ . Penetrating the film towards the substrate, two doublets appear for the component Zr 3d spin-orbit binding energies of  $ZrO_2$  and  $ZrO_xN_y$  simultaneously; penetrating the coating it is predominantly  $ZrO_xN_y$  and after cleaning under an  $Ar^+$  atmosphere 90 min the coating composition is constant. Profile for Zr 3d after cleaning under an  $Ar^+$  atmosphere for 97 min is shown in Fig. 8c. Binding energies of Zr  $3d_{3/2}$  (185.3 eV) and  $3d_{5/2}$  (183.0 eV) have been identified by Soerijanto [42] and Wiame [39] in the phase (ZrNO) of zirconium oxynitride, binding energies of Zr  $3d_{3/2}$  (186.8 eV) and  $3d_{5/2}$  (184.2 eV) would be related to  $ZrO_2$ ; this high binding energy for the Zr 3d peak in  $ZrO_2$  is generated by the higher electronegativity in the system O-Zr-O in comparison with the system O-Zr-N. A summary of the signals corresponding to N1s, O1s and Zr3d is presented in Table II.

TABLE II. Binding energy for O1s, N1s and Zr 3d in  $ZrO_xN_y$  (t) films

Chemical species	Binding energies		
	$ZrO_2$	$ZrO_xN_y$	-OH
O1s	529.6	531.0	532
N1s		396.5	
Zr $3d_{5/2}$	184.2	183.0	
Zr $3d_{3/2}$	186.8	185.3	

These results confirm those obtained for oxygen in Fig. 9a, which shows that near the surface signals of  $ZrO_2$  appear, but upon penetrating a few nm, the zirconia signal disappears and only oxynitride is present. In Fig. 9b binding energy at 531.8 eV has been assigned to the species hydroxyl (-OH) on the surface in absence of nitrogen, binding energy at 529.9 eV assigned to the  $ZrO_2$ . Profile for O1s after cleaning under an  $Ar^+$  atmosphere for 97 min is shown in Fig. 9c, this is shown by the signal at 531.4 eV reported by different authors for ZrNO phase [23,38,43,44]. These results are also consistent with the binding energies associated with nitrogen N 1s, which are absent near the surface, and penetrating a few nanometers toward the substrate, binding energy at 396.5 eV remains constant (Fig. 10a). Signal at 529.9 eV assigned to the  $ZrO_2$ .

Figure 10b shows the high resolution spectrum for Fe 2p, with maxima at 710.8 eV for Fe 2p<sub>3/2</sub> and 724.1 eV for component Fe 2p<sub>1/2</sub>. As reported by Grosvenor, *et al.*, [46], superimposing different signals corresponding to Fe (III) and Fe (II) in various environments hinders an unambiguous assignment of observed signals. This reference shows spectra corresponding to different phases of iron with various oxidation states. Based on this information, we can determine that the observed signals are consistent with the presence of Fe in the oxide form (probably  $\alpha$ - or  $\gamma$ - $Fe_2O_3$ ) or oxo-hydroxide ( $\alpha$ - or  $\gamma$ - $FeOOH$ ). Fe 2p signals, in any case, confirm the oxidation of the substrate.

The formation of oxynitrides at 1023 K obtained by spray pyrolysis-nitriding in a continuous process at atmospheric

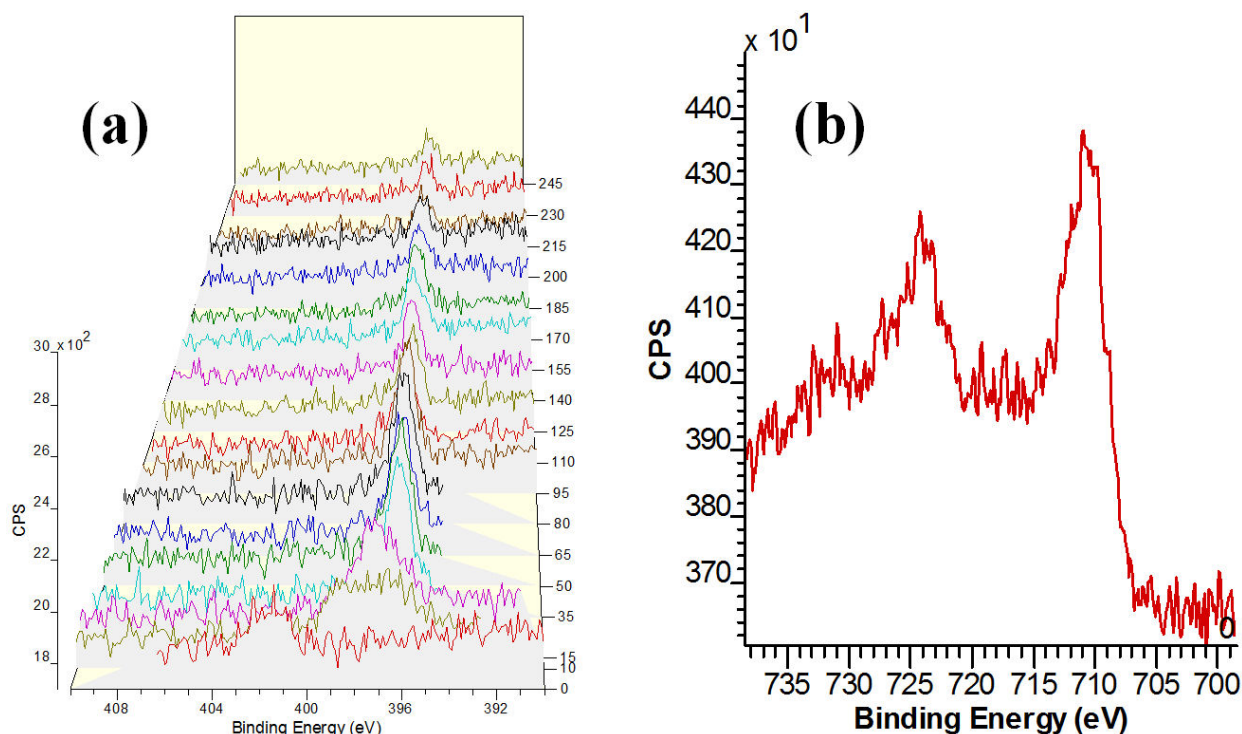


FIGURE 10. High-resolution XPS spectral analysis for the (a) depth profile N1s and (b) Fe 2p in  $ZrO_xN_y$  (t) films nitride at 1023 K,  $\Phi$   $NH_3 = 30$  L/min nitriding, time 30 h.

pressure is remarkable. The lowest temperature in bulk reported by Lerch et al. is in the range of 1673–2173 K [21,22], which shows that the diffusion of nitrogen into a thin film requires less energy, possibly because a thin film facilitates the diffusion of nitrogen toward the anion vacancies of zirconia partially stabilized with yttria. This process has been reported by Soerijanto on the surface of catalysts [42]. As in previous results reported by Lerch [22], the chemical composition of the oxynitride formed is very sensitive to small variations in the conditions for obtaining it, and the coating surface is oxidized to  $ZrO_2$ , but a few nm immediately below the layer of zirconia, an oxynitride layer appears, as the results of the XPS show.

#### 4. Conclusions

The conditions of temperature, time, and flow of anhydrous ammonia were standardized in order to obtain thin films of zirconium oxynitride using the method of *spray pyrolysis-*

*nitriding*. The crystal structure of the deposited material determined from X-ray diffraction and Rietveld refinement was rhombohedral  $Zr_7O_8N_4$ . There was no reported synthesis of oxynitride films by this method at 1023 K. Cation positions were identified, similar to those of  $Ce_7O_{12}$  by Rietveld refinement.

#### Acknowledgments

The authors wish to thank the Foundation for the Promotion of Research and Technology - Bank of the Republic of Colombia, the Directorate for Investigation of the National University of Colombia (DIB) Bogota-Colombia and Iberoamericans Universities post graduate Association (AUIP) for research funding.

1. M. W. Finnis, *Journal of Physics Condensed Matter*. **8** (1996) 5811.
2. J. Hong, T. Chun, and G. Ping, *Surface & Coatings Technology*. **206** (2011) 107.
3. S.C. Ferreira, E. Ariza, L.A. Rocha, J.R. Gomes, and P. Carvalho, *Surface & Coatings Technology*. **200** **2006** 6634.
4. P. Carvalho, F. Vaz, L. Rebouta, L. Cunha, C. Tavares, and C. Moura, *Journal of Applied Physics*. **98** (2005) 023715-1.
5. S. Gutzov, and M. Lerch, *Optical Materials* **24** (2003) 547.
6. N. Fripiat, R. Conaneq, R. Marchand, Y. Laurent and P. Grangea, *Journal of the European Ceramic Society*. **17** **1997** 2011.

7. R. Caruso, B. Gómez, O. De Sanctis, and J. Feugeas, A. Díaz-Parralejo, F. Sánchez, *Thin Solid Films*. **468** (2004) 142.
8. S. Chang and R. Doong, *J. Phys. Chem. B*. **108** (2004) 18098.
9. Y. Song, S. Tsai, C. Chen, T. Tseng, C. Tsai, J. Chen, and Y. Yao, *J. Am. Ceram. Soc.* **87-10** (2004) 1864.
10. M. García *et al.*, *Solid State Ionics*. **179** (2008) 243.
11. X. Youguo, H. Zhaohui, L. Yan-gai, F. Minghao, Y. Li, and G. Ming, *Solid State Sciences*. **14** (2012) 730.
12. M. Tisza, *Physical metallurgy for engineers*. (ASM International and Freund publishing house Ltd., USA., 2002) p. 65-70,.
13. M. Lerch, F. Krumeichb, and R. Hock, *Solid State Ionics*. **95** **1997** 87.
14. J. Chevalier, and L. Gremillard, *J. Am. Ceram. Soc.* **92-9** (2009) 1901.
15. A. S. Foster, V. B. Sulimov, F. Lopez, A. L. Shluger, and R. Nieminen M., *Physical review*. **64** (2001) 224108-1.
16. J.S. Lamas, W.P. Leroy, and D. Depla, *Thin Solid Films*. **525** (2012) 6.
17. J. Hong, Z. En Tsai, and G. Ping, *Surface & Coatings Technology*. **202** (2008) 4992.
18. R. Marchand, Y. Laurent, J. Guyader, P. Haridon, and P. Verdier, *Journal of the European Ceramic Society*. **8** (1991) 197.
19. R. Franchy, *Surface Science Reports*. **38** (2000) 195.
20. L. Bois, P. Haridon, H. Wiame, and P. Grange, *Materials Research Bulletin*. **33** (1998) 9.
21. M. Lerch, *et al*, *Progress in Solid State Chemistry*. **37** (2009) 81.
22. M. Lerch, *Journal of American Ceramic Society*. **79** (1996) 2641.
23. Y. Ohashi, T. Motohashi, Y. Masubuchi, T. Moriga, and K. Murai, S. Kikkawa, *Journal of Solid State Chemistry*. **184** (2011) 2061.
24. I. Cubillos, J. Olaya, M. Bethencourt, G. Cifredo, and J.F. Marco, *Rev. LatinAm. Metal. Mat.* **116** (2013) 33-1.
25. J. Rodríguez, *Physica B: Physics of Condensed Matte*. **1993**, 192, 55.
26. Y. Qiu, L. Gao, *Journal of the European Ceramic Society* **2003**, 23, 2015.
27. G. Istrati, *Manual de los aceros inoxidable*, (Editorial Alsina, Buenos Aires Argentina, 1961).
28. M. Lerch, F. Krumeichb, and R. Hock, *Solid State Ionics*. **95** (1997) 87.
29. Y. Qiu, and L. Gao, *Journal of the European Ceramic Society*. **23** (2003) 2015.
30. F. Bayoumi and W. Ghanem, *Materials Letters*. **59** (2005) 3311.
31. E.A. Kemmerle and G. Heger, *Journal of Solid State Chemistry*. **147** (1999) 485.
32. T. Delachauxa, Ch. Hollensteina, F. Lévyb, and C. Verdonc, *Thin Solid Films*. **425** (2003) 113.
33. A.D. Mazzoni, and E.F. Aglietti, *Materials Chemistry and Physics*. **65** (2000) 166.
34. A. Roustila, J. Chene, and C. Séverac, *Journal of Alloys and Compounds* **330** (2003) 356–357.
35. I. Espitia-Cabrera, H.D. Orozco-Hernández, P. Bartolo-Pérez, and M.E. Contreras-García, *Surface & Coatings Technology*. **203** (2008) 211.
36. A. Roustilaa, J. Cheneb, and C. Severacb, *International Journal of Hydrogen Energy*. **32** (2007) 5026.
37. F. Samanipoura, M.R. Bayatia, F. Golestani-Farda H.R. Zargard, T. Troczynskid, and A.R. Mirhabibia, *Colloids and Surfaces B: Biointerfaces*. **86** (2011) 14.
38. I. Milosev, H. Strehbtow, M. Gaberscek, and B. Navinsek, *Thin Solid Films*. **303** (1997) 246-254.
39. H. Wiame, M.A. Centeno, S. Picard, P. Bastians, and P. Grange, *Journal of the European Ceramic Society*. **18** (1998) 1293.
40. A. Rizzo, M.A. Signore, L. Mirengghi, and T. Di Luccio, *Thin Solid Films*. **517** (2009) 5956.
41. D. Roman *et al.*, *Materials Chemistry and Physics*. **2011**, 130, 147.
42. H. Soerijanto, C. Rodel, U. Wildb, M. Lerch, R. Schomacker, R. Schlögl, and T. Ressler, *Journal of Catalysis*. **250** (2007) 19.
43. M. Chan, P. Wu, and F. Lu, *Thin Solid Films*. **518** (2010) 7300.
44. M.A. Signore, A. Rizzo, L. Mirengghi, M.A. Tagliente, and A. Cappello, *Thin Solid Films*. **515** (2007) 6798.
45. NIST X-ray Photoelectron Spectroscopy Database, *NIST Standard Reference Database 20*, (Version 3.5. copyright by the U.S. Secretary of Commerce on behalf of the United States of America, 2003).
46. A. P.Grosvenor, B. A. Kobe, M. C. Biesinger, and N. S. McIntyre, *Surf. Interface Anal.* **36** (2004) 1564.